Quantitative phase contrast imaging of THz electric fields in a dielectric waveguide

Citation: Wu, Qiang, Christopher A. Werley, Kung-Hsuan Lin, August Dorn, Moungi G. Bawendi, and Keith A. Nelson. "Quantitative phase contrast imaging of THz electric fields in a dielectric waveguide." Optics Express 17, no. 11 (May 15, 2009): 9219.© 2009 Optical Society of America.

As Published: http://dx.doi.org/10.1364/OE.17.009219

Publisher: Optical Society of America

Persistent URL: http://hdl.handle.net/1721.1/81890

Version: Final published version: final published article, as it appeared in a journal, conference proceedings, or other formally published context

Quantitative phase contrast imaging of THz electric fields in a dielectric waveguide

Qiang Wu[1,2*], Christopher A. Werley[1], Kung-Hsuan Lin[1,3], August Dorn[1], Moungi G. Bawendi[1], and Keith A. Nelson[1†]

[1]Department of Chemistry, Massachusetts Institute of Technology, Cambridge, Massachusetts 02139, USA
[2]The Key Laboratory of Weak Light Nonlinear Photonics, Ministry of Education, Physics Institute, and TEDA Applied Physics School, Nankai University, Tianjin 300457, P. R. China
[3]Laser Application Technology Center, Industrial Technology Research Institute South, Liujia Shiang 73445, Taiwan
**Corresponding author: wuqiang@nankai.edu.cn*
†Corresponding author: kanelson@mit.edu

Abstract: We apply phase contrast imaging to enable, sharply focused visualization of terahertz waves in electro-optic media. The approach allows quantitative characterization of THz waves in the 60 GHz – 4.5 THz frequency range in a thin dielectric slab and in-focus observation of THz waves in polaritonic structures.

OCIS codes: (040.2235) Far infrared or terahertz; (320.7150) Ultrafast spectroscopy; (300.6495) Spectroscopy, terahertz; (110.6760) Talbot and self-imaging effects; (040.2840) Heterodyne; (070.4550) Correlators.

References and links

1. T. Feurer, N. S. Stoyanov, D. W. Ward, J. C. Vaughan, E. R. Statz, and K. A. Nelson, "Terahertz Polaritonics," Annu. Rev. Mater. Res. **37**, 317-350 (2007).
2. T. P. Dougherty, G. P. Wiederrecht, and K. A. Nelson, "Impulsive stimulated Raman scattering experiments in the polariton regime," J. Opt. Soc. Am. **9**, 2179-2189 (1992).
3. D. Auston and M. Nuss, "Electrooptic Generation and Detection of Femtosecond Electrical Transients," IEEE J. Quantum Electron. **24**, 184-197 (1988).
4. A. G. Stepanov, J. Kuhl, I. Z. Kozma, E. Riedle, G. Almási, and J. Hebling, "Scaling up the energy of THz pulses created by optical rectification," Opt. Express **13**, 5762-5768 (2005).
5. K. –L. Yeh, M. C. Hoffmann, J. Hebling, and Keith A. Nelson, "Generation of 10 μJ ultrashort terahertz pulses by optical rectification," Appl. Phys. Lett. **90**, 171121 (2007).
6. T. Feurer, N. S. Stoyanov, D. W. Ward, and K. A. Nelson, "Direct Visualization of the Gouy Phase by Focusing Phonon Polaritons," Phys. Rev. Lett. **88**, 257402 (2002).
7. T. Feurer, J. C. Vaughan, and K. A. Nelson, "Spatiotemporal Coherent Control of Lattice Vibrational Waves," Science **299**, 374-377 (2003).
8. N. S. Stoyanov, D. W. Ward, T. Feurer, and K. A. Nelson, "Terahertz polariton propagation in patterned materials," Nature Materials **1**, 95-98 (2002).
9. N. S. Stoyanov, T. Feurer, D. W. Ward, and K. A. Nelson, "Integrated diffractive terahertz elements," Appl. Phys. Lett. **82**, 674-676 (2003).
10. J. P. Wolfe, *Imaging phonons: acoustic wave propagation in solids* (Cambridge University Press, Cambridge, 1998).
11. Q. Wu, T. D. Hewitt, and X.-C. Zhang, "Two-dimensional electro-optic imaging of THz beams," Appl. Phys. Lett. **69**, 1026-1028 (1996).
12. Z. Jiang and X.-C. Zhang, "Terahertz Imaging via Electrooptic Effect," IEEE Trans. Microwave Theory Tech. **47**, 2644-2650 (1999).
13. R. M. Koehl, S. Adachi, and K. A. Nelson, "Direct Visualization of Collective Wavepacket Dynamics," J. Phys. Chem. A **103**, 10260-10267 (1999).
14. D. W. Ward, E. R. Statz, K. A. Nelson, R. M. Roth, and R. M. Osgood, "Terahertz wave generation and propagation in thin-film lithium niobate produced by crystal ion slicing," Appl. Phys. Lett. **86**, 022908 (2005).
15. H. F. Talbot, "Facts relating to optical science no. IV," Philos. Mag. **9**, 401-407 (1836).
16. P. Peier, S. Pilz, F. Müller, K. A. Nelson, and T. Feurer, "Analysis of phase contrast imaging of terahertz phonon-polaritons," J. Opt. Soc. Am. B **25**, B70-B75 (2008).
17. F. Zernike, "How I discovered phase contrast," Science **121**, 345-349 (1955).
18. F. Zernike, "Phase contrast: a new method for the microscopic observation of transparent objects," Physica **9** 686-698 (1942).

#109109 - $15.00 USD Received 23 Mar 2009; revised 25 Apr 2009; accepted 27 Apr 2009; published 15 May 2009

19. Joseph W. Goodman, *Introduction to Fourier Optics, 3rd edition* (Roberts & Company Publishers, Englewood, 2005), Chap. 8.
20. N. J. Cronin, *Microwave and Optical Waveguides* (Institute of Physics Publisher, Philadelphia, 1995).
21. D. W. Ward, E. R. Statz, and K. S. Nelson, "Fabrication of polaritonic structures in $LiNbO_3$ and $LiTaO_3$ using femtosecond laser machining," Appl. Phys. A **86**, 49-54 (2007).
22. Joseph W. Goodman, *Introduction to Fourier Optics, 3rd edition* (Roberts & Company Publishers, Englewood, 2005), Chap. 5.

Terahertz frequency phonon polariton waves can be efficiently generated by femtosecond laser pulses in ferroelectric crystals such as lithium niobate (LN) [1,2]. At frequencies less than ~2 THz, they behave primarily like electromagnetic waves and propagate with minimal dispersion at light-like speeds through the host material. The THz radiation can be coupled into free space [3], and this has been one of the primary methods for high-amplitude THz generation [4, 5]. The THz can also be manipulated directly within a THz slab where a diverse set of generation capabilities has already been demonstrated, including THz focusing [6], shaping, and amplification [7]. Further manipulation of these waves with various types of structures such as interferometers [8] and gratings [9] has also been demonstrated. For many of the effects above, both spatial and temporal information is important, making time-resolved imaging a powerful tool for studying these phenomena. Time-resolved imaging of phonons has been a key in elucidating a host of effects in solids for a number of decades [10], and has more recently been applied to THz electromagnetic fields [11, 12]. Phonon polariton waves were first imaged in LN in 1999 [13]. In LN, the THz waves are generated in a Cherenkov pattern, and because the 800 nm group velocity is roughly 2.3 times the THz phase velocity, they propagate through the crystal nearly perpendicular to the optical beam that generates them (see Fig. 1(b)) [1, 3]. The optical probe travels nearly collinear with the pump, yielding a "side view" of the THz pulse which shows spatial field oscillations, which has facilitated many of the experiments mentioned above [6-9, 13, 14]. However, previous phonon-polariton imaging has not yielded quantitative characterization of broadband field profiles or sharp, in-focus view of polaritons and the structures in which they propagate.

In general, the THz wave is launched by an intense pump beam and imaged with an expanded probe. Because LN has large electrooptic coefficients, the index of refraction is strongly modulated by the THz electric field. As the plane wave of the probe passes through the crystal it develops a phase shift proportional to the electric field, leading to a phase image immediately after the sample. Previously this has usually been visualized using the Talbot effect [6-9, 13, 14], where a phase image is converted to an amplitude image by translating the camera out of the image plane of the sample [15]. Using Fresnel diffraction theory, it has been shown that a phase grating pattern with period d imposed on a plane wave of wavelength λ is completely converted into an amplitude grating after a propagation distance $d^2/2\lambda$ [13]. Thus for a camera translated out of the image plane some phase information will be converted to amplitude information, but only certain wave vector components of the phase image will be efficiently detected, which makes quantitative E-field measurement impossible. Another drawback of the Talbot method is that static structures in the sample will be blurred because the CCD camera is not in the image plane. Recently, Peier *et al* [16] investigated the wave vector response of Talbot imaging, and demonstrated two new methods, Sagnac interferometry and polarization gating, that address this problem. Sagnac imaging has significant drawbacks when working with structured crystals and polarization gating requires a compensating crystal, which only works well when samples have extremely uniform thicknesses. In this paper we demonstrate quantitative measurement of THz electric fields and in-focus imaging of static structures with time-resolved phase contrast imaging, which addresses the deficiencies of Talbot imaging but avoids issues inherent to Sagnac imaging and polarization gating.

Phase contrast imaging was first introduced by Frits Zernike in the 1930s [17,18] and has been widely used in biology for imaging cells and other transparent specimens since then. Here we use a two-lens imaging system with a phase plate at the center focal plane, i.e. a 4*f* correlator, to implement this technique. In brief, in the back focal plane of the first lens (the

#109109 - $15.00 USD Received 23 Mar 2009; revised 25 Apr 2009; accepted 27 Apr 2009; published 15 May 2009

Fourier plane) there is spatial separation between the undeflected or "0th order" beam, which is focused at the center, and the diffracted light, which is spread throughout the plane (see Fig. 1(a)). The phase plate takes advantage of this spatial separation by inducing a π/2 relative phase shift between the 0th order beam and the diffracted light. The 0th order beam and diffracted light recombine in the image plane of the second lens where they interfere because of the induced phase shift, bringing about phase to amplitude conversion.

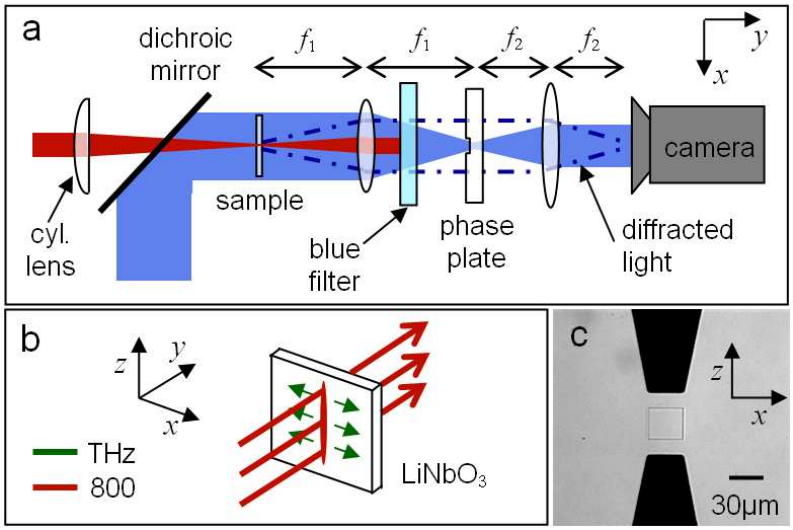

Fig. 1. Experimental setup. (a) Schematic diagram. The sample, a 53 μm slab of $LiNbO_3$, is imaged onto the camera using two lenses, and the phase plate is placed in the Fourier plane of the first lens. The 800 nm pump (red) and 400 nm probe (blue) are nearly collinear when they hit the sample. In our setup, $f_1 = f_2 = 15$ cm. (b) The pumping geometry. The 800 nm beam propagates through the crystal, orthogonal to its surface, polarized along *z*. The THz response, also polarized along *z*, propagates in the plane of the waveguide. (c) A bright-field image of the phase plate. The depressed square is 30 um across and 215 nm deep. The metal arrows (black in the Fig. 1 (c)) aid in alignment.

The phase plates were fabricated using double sided optical flats (±0.016 wave) made of fused silica (SYDOR Optics) with a surface area of 25x25 mm and a thickness of 2mm. A 215±5 nm layer of 950 kDalton PMMA from MicroChem (n ~ 1.52 at 400 nm) was spin coated onto the substrates and a 30x30 μm area in the center of the plate was developed using electron beam lithography and removed. This led to phase plates with an extremely flat surface that were transparent in the visible with a central square recessed by 215±5 nm, ~$\lambda/4$ for the 400 nm probe wavelength (see Fig. 1(c)). Gold arrows (black in the Fig. 1(c)) with a 60-μm gap were deposited to assist in the alignment of the phase plate in the optical setup. For some samples or experimental setups these could block diffracted light. However, for the work presented here the diffracted information is spread only along the *x*-axis because of the near-uniformity of the THz wave along the *z*-axis resulting from excitation with a cylindrical lens.

We used a Ti:sapphire femtosecond laser system with a central wavelength of 800 nm, a repetition rate of 1 KHz and a pulse duration of about 70 fs. The laser output is split into pump (400 μJ) and probe (frequency-doubled, 400 nm, 1 μJ) pulses which can be delayed relative to one another. The pump is focused into the sample using a cylindrical lens, which acts as a line source for THz radiation. The probe is spatially filtered and expanded to obtain a large spot with minimal spatial variation before passing through the crystal. The crystal is imaged onto a Princeton Instruments PIXIS camera using 15 cm focal length achromatic lenses. For optimum signal, the polarizations of the pump, probe, and THz fields are all parallel to the extraordinary axis of the LN [1].

#109109 - $15.00 USD Received 23 Mar 2009; revised 25 Apr 2009; accepted 27 Apr 2009; published 15 May 2009

Figure 2(a) shows a picture captured using phase contrast imaging of a THz wave in an unstructured, 53-μm dielectric slab waveguide 42 ps after it was generated with a line focus (see (Media 1)) for full temporal evolution). Because the slab is thin relative to the THz wavelength, the light is broken up into discrete waveguide modes, the first three of which are visible.

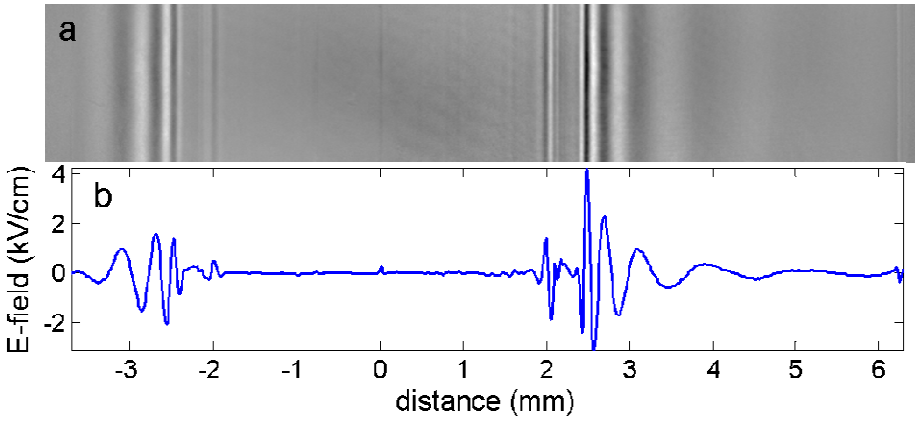

Fig. 2. (a) (Media 1) Image of a THz field in a 53-μm LN crystal slab 42 ps after excitation by a cylindrically focused pump pulse. The chirping of the pulse because of waveguide dispersion and the first three waveguide modes are apparent. (b) The field profile from (a), averaged over the vertical dimension. Initial field strengths are higher but dispersion quickly broadens the pulse and lowers peak field amplitudes.

The THz pulse shows significant chirp which results from the strong geometrical dispersion experienced by the waveguide modes. It is possible to quantitatively measure the THz fields in the image. As the probe propagates through the crystal, the THz field induces a relative phase shift:

$$\Delta\phi_{\text{opt}}(x,z) = 2\pi\frac{\ell}{\lambda_{\text{opt}}}\Delta n(x,z) = 2\pi\frac{\ell}{\lambda_{\text{opt}}}\frac{n_{eo}^3 r_{33}}{2}E_{\text{THz}}(x,z) \tag{1}$$

where ℓ is the slab thickness, λ_{opt} is the probe wavelength, n_{eo} is the extraordinary index of refraction of LN for the probe, and r_{33} is the electrooptic coefficient [1]. E_{THz} is the average THz field experienced by the probe pulse as it propagates through the crystal in the y direction. As the probe propagates through the crystal the THz field is also propagating, but more slowly due to the higher index and in an orthogonal direction. For the lowest waveguide mode, E_{T} is close to (but less than) the maximum field inside the crystal. Thus the measured field strength calculated using Eq. (1) serves as an estimate (and lower bound) to the actual maximum field. The second waveguide mode has a node along y in the central plane of the crystal. As the probe propagates through the crystal, the phase shift introduced by the positive and negative lobes of the THz field tend to cancel, so for the same peak THz field strength a smaller phase shift is introduced in the second mode relative to the first. Before we can use Eq. (1) to learn about the THz E-fields, it is first necessary to quantitatively measure the phase, $\Delta\phi_{\text{opt}}(x,z)$. For an ideal $\lambda/4$ phase plate, to first order in the THz-induced phase shift, the measured signal from phase-contrast imaging is:

$$I(x,z) = I_0(x,z)[1-2\Delta\phi(x,z)] \tag{2}$$

with $I_0(x,z)$ the intensity envelope of the optical probe beam [19]. Thus we can extract the phase *in silico* by the operation:

#109109 - $15.00 USD Received 23 Mar 2009; revised 25 Apr 2009; accepted 27 Apr 2009; published 15 May 2009

$$\Delta\phi_{\text{opt}}(x,z) = \frac{1}{2}\left(1 - \frac{S(x,z)}{R(x,z)}\right) = -\frac{1}{2}\frac{\Delta I(x,z)}{I_0(x,z)} \tag{3}$$

were $S(x, z)$ is the signal image intensity and $R(x, z)$ is the reference image intensity measured with the pump blocked. Equation (1) can then be used to calculate the electric field. Figure 2(b) shows the quantitative field profile, calculated by averaging over the vertical dimension of the image in Fig. 2(a).

Because the sample in Fig. 2(a) (Media 1) is a simple, unstructured dielectric slab waveguide, we can easily compare the measured dispersion characteristics with theory. To compact our data, we averaged over the vertical dimension (as was done to calculate Fig. 2(b)) for each time step in (Media 1) and placed the resulting vector in one row of a matrix. In this way the full temporal and spatial evolution in the slab waveguide can be displayed in one image, as shown in Fig. 3(a). In this image, dispersion, reflection, interference, and the different waveguide modes are all clearly apparent. By taking the 2-dimensional Fourier transform of this image, we get the dispersion curve of the system, shown in Fig. 3(b). The horizontal axis is the propagation constant, β, with $\beta = k_x$ for the axes defined in Fig. 1(b).

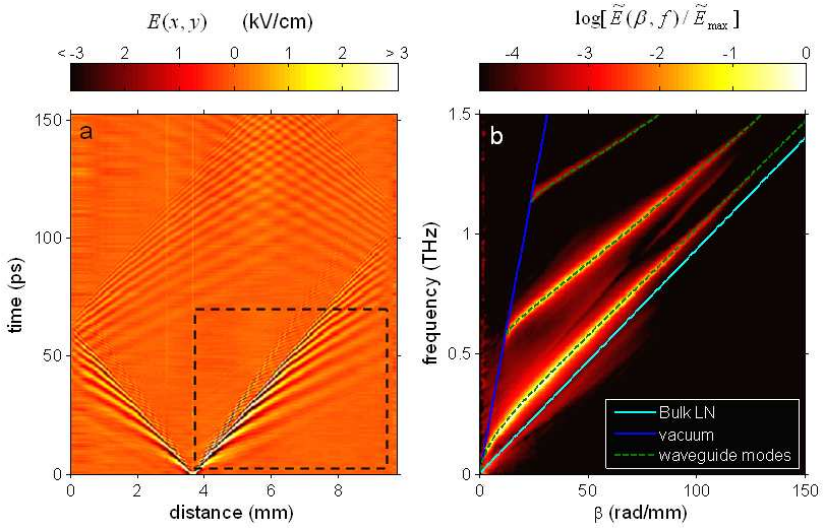

Fig. 3. (a) E-field evolution as a function of space and time. The sides of the image correspond to the edges of the crystal. The colorbar has been scaled to enhance weaker signals; the maximum field strength at early times exceeds 10 kV/cm. (b) One quadrant of the 2D Fourier transform of the boxed region in (a). This gives the dispersion curve with the propagation constant β along the horizontal axis ($\beta = k_x$ for the coordinate system shown in Fig. 1(b)). The colorbar gives the normalized spectral intensity on a log scale. The first three waveguide modes are clearly visible. Overlaid on the experimental data are the theoretical dispersion curves for air (dark blue), bulk lithium niobate (light blue) and the first three waveguide modes for a 53 um slab (dashed green). There were no free parameters in this theoretical model.

Each waveguide mode above displays a unique dispersion curve, and shows expected behaviors such as distinct nonlinear behavior near the free-space light line and cutoff frequencies for the higher modes. Overlaid on top of the experimental dispersion curves in dashed green are the theoretical dispersion curves [20] for a 53 μm slab, where we used the frequency dependent index of refraction from [1]. The calculated dispersion curves for air and bulk LN are shown as solid lines for a reference. There were *no* fit parameters, although a 2% rescaling of the experimental wave vector axis was necessary. This is a change well within the uncertainty of our length calibration. The excellent agreement between experimental and theoretical results demonstrates that phase contrast imaging can accurately record spatial phase profiles. A similar dispersion curve measured with Talbot imaging, such as Fig. 14(h)

#109109 - $15.00 USD Received 23 Mar 2009; revised 25 Apr 2009; accepted 27 Apr 2009; published 15 May 2009

of ref. [1], will have nodes along specific wave vectors determined by the camera location instead of the flat response of phase contrast imaging.

The quantitative determination of THz E-fields in highly structured materials presents additional challenges. Low wave vector light diffracted off of relatively large, static structures in the sample may be poorly separated from the 0^{th} order beam in the Fourier plane of the first lens. As a result, some of the light may scatter off of the sharp edges of the depression in the phase plate. This leads to imperfect reconstruction in the image plane: the smooth intensity profile of the probe is modulated at the scattered wave vector. This is a fairly small effect, however, and the THz-wave-induced phase information is still 90° with the 0^{th} order beam, so in most cases a good estimate of the THz electric field can still be made. Figure 4 shows an image of the z-component of the THz fields in a structured substrate captured using phase contrast imaging. A Y-coupler was cut into the 53 μm LN slab waveguide (the triangle and angled and straight rectangular boundaries around the "Y" are air, the rest is LN) using femtosecond laser machining [21]. In this sample a vertically uniform, rightward propagating THz wave was incident on the right side of the Y-coupler. Two components of the wave were guided down the arms of the Y, and in Fig. 4 they can be seen interfering at the intersection. The THz wave can be clearly observed with high contrast and the structure itself is clear and in focus, which was not possible using previous techniques [6-9, 13, 14]. Please see (Media 2) online for more details.

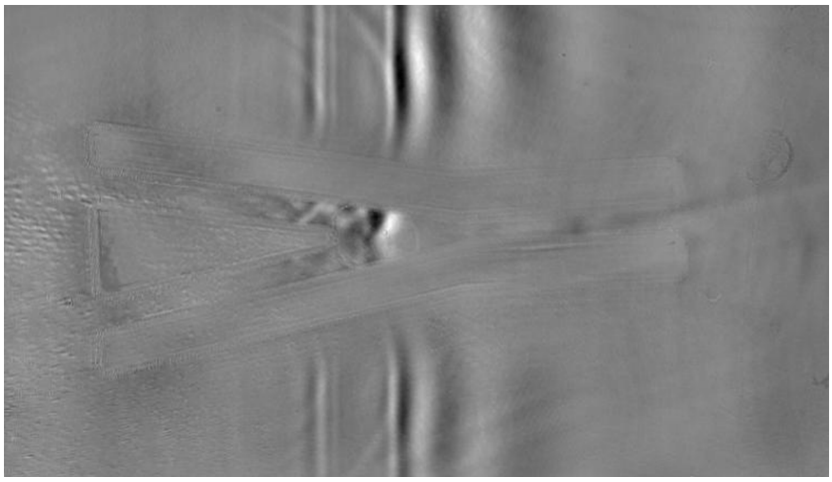

Fig. 4. (Media 2) The z-component of the THz E-field in a structured, 53 μm LN substrate.

This technique has some limitations on its detection bandwidth. On the low-frequency side, if the diffracted light passes through the depression in the phase plate, it will not be converted to an amplitude pattern in the image plane. Using the formalism of Fourier optics, the complex field of the optical probe in the back focal plane of the first lens (the plane where the phase plate resides; see Fig. 1(a)) is given by:

$$u(x,z) = U_0(k_x, k_z)\,|_{k_x = 2\pi x/\lambda f,\ k_z = 2\pi z/\lambda f} \tag{4}$$

with f the focal length of the lens, λ the probe wavelength, and $U_0(k_x, k_z)$ the 2D Fourier transform of the complex optical field right after the sample, $u_0(x,z)$ [22]. Given our experimental parameters (f = 15 cm, λ = 400 nm, depression size = 30 x 30 μm), the edge of the depression corresponds to a THz wave vector of 1.6 rad/mm, a wavelength of 4 mm. The numerical aperture of our system (NA ~ 0.08) is sufficient to resolve feature sizes larger than about 3 μm. Thus for our choice of lens and phase plate we can detect phase objects with feature sizes from 3 μm – 4 mm, and even shorter wavelengths can be detected if a shorter focal length lens is used, although this happens at the expense of long-wavelength cutoff. For

#109109 - $15.00 USD Received 23 Mar 2009; revised 25 Apr 2009; accepted 27 Apr 2009; published 15 May 2009

the lowest waveguide mode of a 53 μm $LiNbO_3$ slab, this corresponds to a frequency bandwidth of ~60 GHz to 20 THz. For the purpose of detecting THz waves in a thin LN slab, the high-frequency cutoff is actually limited not by the imaging system but because we do not employ phase matched detection. As the probe pulse propagates through the slab, it accumulates phase proportional to THz field, which is also propagating but in an orthogonal direction (Fig. 1). For low THz frequencies this is a small effect and the optical pulse sees essentially the same field the whole time it is interacting with the slab, but high THz frequency signals are rapidly varying and tend to get smeared out. For the lowest waveguide mode in a 50 μm slab, this effect cuts off detection at ~3 THz; in a 30 μm slab, the cutoff is extended to ~4.5 THz.

Although our current setup is sensitive enough to detect many phenomena of interest, further improvements are possible through control of both the amplitude and phase of the 0^{th} order beam. If in addition to introducing a phase shift of π/2, the central 30x30 μm square were also partially reflective and attenuated the 0^{th} order beam amplitude by a factor of a $(0 < a < 1)$, then Eq. 2 would be modified to $I(x,z) = I_0(x,z)[a^2 + 2a\Delta\phi(x,z)]$. Although the signal itself is weakened by a factor of a, the background is reduced by a factor a^2, which improves the signal to noise ratio by a factor of $1/a$ [18], assuming shot-to-shot laser fluctuations are the primary noise source in the experiment. The weakened signal can be compensated by increasing the probe intensity and/or the camera integration time. If an appropriate phase plate can be fabricated, it should be possible to achieve 3-fold or better improvements in signal to noise using this method.

We have demonstrated that phase contrast imaging provides high sensitivity for visualization and quantitative evaluation of THz phonon-polariton waves in electro-optic crystals. The method enables detection over a phonon-polariton wavelength range spanning more than two decades and a corresponding frequency range of nearly two decades. It allows us to quantitatively resolve electric fields both spatially and temporally in structured or unstructured waveguides, thus exposing the details of phonon-polariton wave evolution. These capabilities will be extremely useful for future studies of patterned samples such as metamaterials or photonic crystals and for the general advancement of polaritonics. It should be noted that the technique can be used to study other phenomena in which the index of refraction is modulated spatially and temporally. For example, we have observed phonons in lithium niobate that change the index via acousto-optic effect.

Acknowledgments

This work was supported in part by National Science Foundation Grant No. ECCS-0824185, a National Science Foundation Graduate Research Fellowship (C.A.W.), and a National Natural Science Foundation of China Grant No. 10604033. K.-H. Lin would like to thank National Science Council of Taiwan under NSC-095-SAF-I-564-614-TMS.

#109109 - $15.00 USD Received 23 Mar 2009; revised 25 Apr 2009; accepted 27 Apr 2009; published 15 May 2009